Paleo-aridity records investigated through drip water chemistry in Lehman Caves, Nevada

by

Rory S. Knight

Submitted to the Department of Earth, Atmospheric, and Planetary Sciences
in partial fulfillment of the requirements for the degree of

BACHELOR OF SCIENCE IN EARTH, ATMOSPHERIC, AND PLANETARY SCIENCES

at the

MASSACHUSETTS INSTITUTE OF TECHNOLOGY

May 2025

Authored by: Rory S. Knight
Department of Earth, Atmospheric, and Planetary Sciences
May 9, 2025

Certified by: David McGee
Professor of Earth, Atmospheric, and Planetary Sciences, Thesis Supervisor

Accepted by: Taylor Perron
Professor of Earth, Atmospheric and Planetary Sciences
Undergraduate Officer, Department of Earth, Atmospheric and Planetary Sciences

Paleo-aridity records investigated through drip water chemistry in Lehman Caves, Nevada

by

Rory S. Knight

Submitted to the Department of Earth, Atmospheric, and Planetary Sciences on May 9, 2025 in partial fulfillment of the requirements for the degree of

BACHELOR OF SCIENCE IN EARTH, ATMOSPHERIC, AND PLANETARY SCIENCES

ABSTRACT

In the Great Basin of the southwest United States, climate change is predicted to cause increased precipitation variability, making the future climate of the region uncertain. The paleoclimate record has direct examples of dramatic changes in water availability in this area, allowing for a comparison of precipitation changes and responses for the Great Basin. In Lehman Cave, Nevada, ten drips above actively-forming stalagmites were sampled monthly. Glass growth plates were also placed above three actively-forming stalagmites, allowing for the collection of new calcite growths. This project analyzed the samples for Mg/Ca, Sr/Ca, and U/Ca ratios to provide a comparison of the composition of calcite and the drip waters from which they precipitate. This will improve our understanding of the paleo-aridity of the Great Basin region, as well as provide useful context for the changing precipitation patterns expected with modern climate change.

Thesis supervisor: David McGee
Title: Professor of Earth, Atmospheric, and Planetary Sciences

Acknowledgments

This research could not have been completed without the help of many individuals. Firstly, I would like to thank my advisor, Professor David McGee, for his incredible support and assistance throughout this project. I could not have asked for a more supportive, patient, and knowledgeable mentor. I am also grateful to the rest of the McGee Lab, particularly Adam Jost and Madi Wittmer, for their help in this project. Thank you to Gretchen Baker and the staff of Great Basin National Park, who collected samples used for this project and facilitated many aspects of this work.

Outside of the lab, my wonderful friends on Tetazoo and Black Hole provided significant emotional support throughout the process of writing this thesis, particularly Eugeniya Artemova, Alexi Stewart, and Lev Romashkov. Thank you to Ray Feller from Student Support Services, who has been an incredible support person since my freshman year. Finally, I would like to thank the EAPS Department as a whole, for providing a community that encourages me to explore the universe, on Earth and beyond.

Contents

List of Figures

Chapter 1

Introduction

1.1 Previous Studies

The precise timing of hydrological changes in the Great Basin in the early-to-mid Holocene is not well established, although previous studies have investigated this [1–3]. Prior research into the paleoclimate record in the Great Basin have analyzed lake sediment deposits as well as stalagmite samples [3–7]. The Devils Hole calcite δ^{18}O record from the Great Basin, Nevada, indicates that there was a deglaciation at 142 $\pm$ 3 ka, while a Lehman Caves stalgmite shows this deglaciation at 133 to 129 ka [4]. Lehman Caves stalagmites indicated a transition from wet to dry conditions from 130 to 128 ka [6]. On a more recent timeline, stable isotope and trace metal data from additional Lehman Caves speleothems have indicated a wetter period from 12.7 to 8.2 ka, with pronounced drying after 8.2 ka [3]. Conversely, lake deposits, as well as fossilized small mammals and plants, indicate increased drying after 11.5 ka, and that the early Holocene was about 3 degrees Celsius cooler than the present. Lake sediments are limited in their temporal resolution, while high precision U-Th dating of speleothems provides a precise chronology for the samples, allowing for the development of detailed timing of wet and dry periods.

Conclusions about past climatic conditions from stalagmite data have been limited in that they indicate wet and dry periods but not how wet or dry the periods were, but recent studies have shown the relevance of Mg/Ca ratios in stalagmites as measurements of paleo-aridity [3, 6]. When water is held in the epikarst, or the layer above the cave, for longer periods due to less recharge from rainfall, the water begins to lose carbon dioxide before reaching the cave. Degassing of CO2 causes calcite to precipitate. This calcite forms in cracks and spaces in the rock in a process called prior calcite precipitation (PCP). Calcium is used to form calcite during PCP, while magnesium is left behind. Therefore, the water reaching the cave that is held in rock for longer periods has a higher Mg/Ca ratio than water that travels quickly from surface to cave. By analyzing the Mg/Ca ratio in calcite that forms in caves, we can identify dry periods in which less recharge and more PCP occurs, giving a higher Mg/Ca ratio in the cave calcite. Therefore, higher Mg/Ca likely indicates a drier period, while lower Mg/Ca signifies a wet period. Strontium is expected to show a similar relationship, leading to higher Sr/Ca values in a drier period and lower Sr/Ca values in a wetter period.

Cave drip waters are critical archives of climate information, particularly through their role in the formation of speleothems. Trace element ratios such as Mg/Ca, Sr/Ca, and U/Ca are sensitive to hydrological and geochemical processes, which can allow them to provide insight into the past climate of the region. By comparing element ratios across seasons and cave rooms, we aim to identify environmental controls on drip water chemistry and assess how these may impact paleoclimate reconstructions.

1.2 Regional Setting

Lehman Caves is located at 39°00’20"N, 114°13’13"W, near the middle of the Nevada-Utah border on the Nevada side, on the edge of the Bonneville Basin (Fig. 1.1). The cave system sits at 2130m of elevation, making it a local topographic high, which causes the majority of the water entering the cave to be from infiltration directly above the cave, not run-off. Winter precipitation is the main source of seasonal recharge, and drip water response time is recorded as 1 to 4 weeks [3].

Figure 1.1: Map of the Great Basin (central outline in grey) with Lehman Caves marked (red circle). Basemap sourced from Esri, USGS | Esri, TomTom, Garmin, FAO, NOAA, USGS, EPA, USFWS; Great Basin outline sourced from HydroSHEDS. [8].

Chapter 2

Materials and Methods

2.1 Sample Collection

Sixteen locations in Lehman Caves were selected for drip site collection in August 2023. The sites were in multiple locations in the Lodge Room, Inscription Room, West Room, Talus Room, Sunken Garden, and Grand Palace (Fig. 2.1). Drip waters were collected from these sites in four sampling months: August 2023, March 2024, May 2024, and October 2024. Drip rates were also measured at the collection sites during those times, as well as April 2024, June 2024, July 2024, and September 2024, by counting the time elapsed between drips. In three locations, Sites 4, 9, and 14, glass plates were placed under the drip to collect calcite deposits that form over time.

2.2 Sample Analysis

Calcite deposits were scraped off of the sample plates with a drill bit and dissolved in 1.5 ml of 0.5M HNO_3. Drip waters were added to vials with 200 ng/g Sc+In standard. Drip waters and calcite deposits were analyzed for Ca, Mg, Sr, U, Sc, and In using inductively coupled plasma mass spectrometry (ICP-MS) at the Massachusetts Institute of Technology. A calibration curve was made using standards with 0%, 25%, 50%, and 100% water, with a standard concentration of 40.3190378 µg/g Mg, 389.103071 µg/g Ca, 0.57704555 µg/g Sr, and 0.00032463 µg/g U. Every five samples, 50% standards were run to correct for drift.

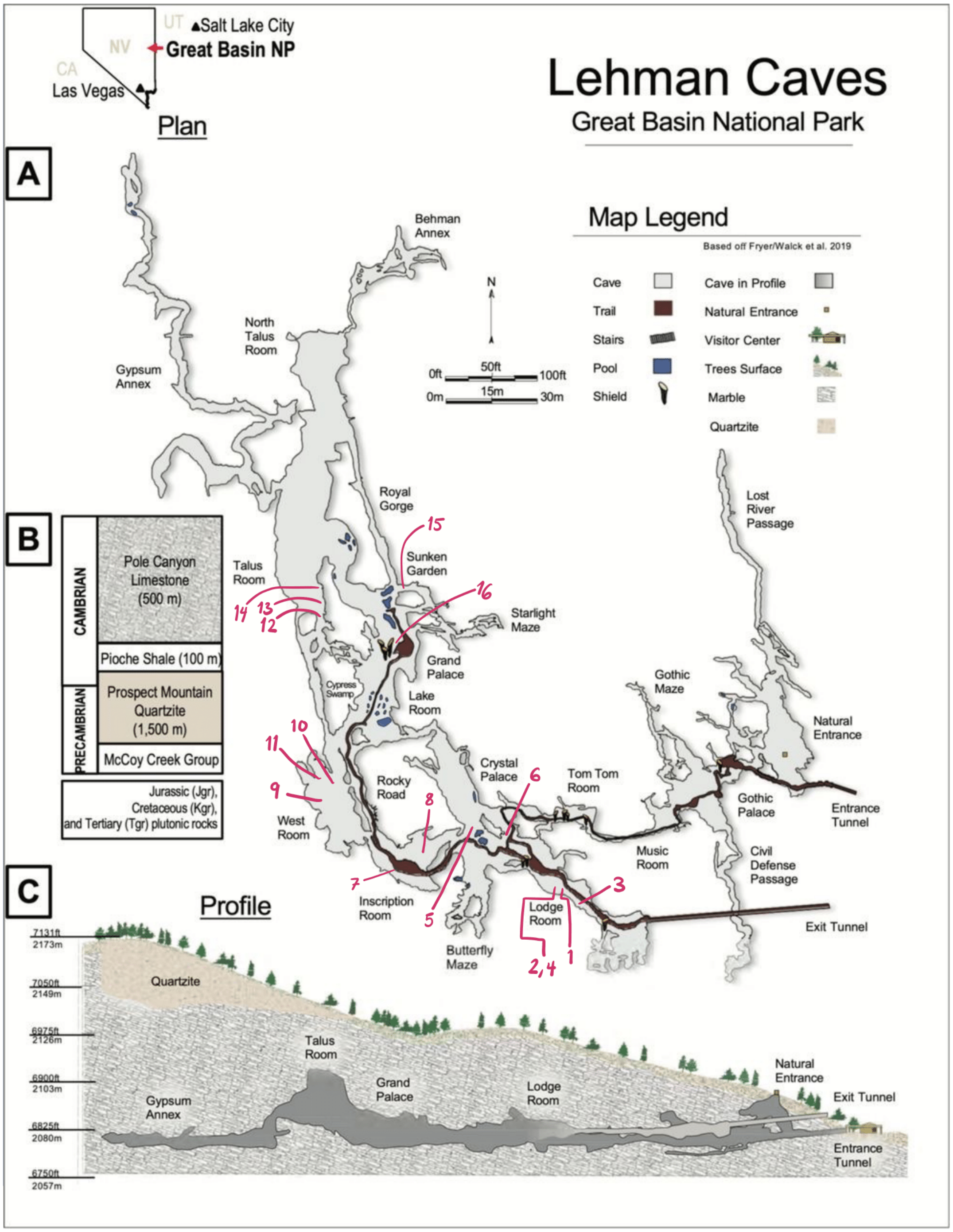

Figure 2.1: Map of Lehman Caves, with sample sites labeled. Basemap sourced from Zoë E. Havlena, et al. (2023). [9].

Chapter 3

Results

3.1 Elemental composition of drip waters and calcite deposits

Mg/Ca of drip waters ranges between approximately 0.07 and 1.59 mol/mol; Sr/Ca is between approximately 0.54 and 6.08 mmol/mol; U/Ca is between approximately 0.19 and 9.51 umol/mol (Fig. 3.1). For the calcite samples, Mg/Ca ranges between approximately 0.89 and 188.64 mmol/mol; Sr/Ca is between approximately 0.23 and 0.54 mmol/mol; U/Ca is between approximately 0.37 and 4.69 umol/mol. Mg/Ca and Sr/Ca show a strong positive correlation (Fig. 3.2).

Measured drip rates range from 0 (dry) to 15 drips per minute, with the highest drip rates recorded as well as the greatest variation in drip rates recorded in March and August (Fig. 3.3).

Environmental parameters such as temperature and precipitation were sourced from the Baker, NV station of Weather Underground, which is placed approximately 2.1 kilometers from the cave entrance. The temperature for the months studied ranged from 40.12°F in March 2024 to 72.23°F in August 2023, and precipitation ranging from 0.09 inches in June 2024 to 1.58 inches in August 2023 [10]. The first set of drip plates was left in place from

August 2023 to March 2024, and the second from March 2024 to October 2024. During the first period of time, Baker, NV received 6.22 inches of rain total, with 3.5 inches of rain collected in the second period [10]. Mg/Ca ratios tend to be lower in the cooler and wetter months and higher in drier, warmer months (Fig. 3.4). For example, in the Grand Palace, Mg/Ca increased from 0.64 mol/mol in August 2023 (a very rainy month) to 1.59 mol/mol in May 2024 (a very dry month). Sr/Ca ratios show similar trends, with higher values in dry months across several sites. U/Ca ratios were more variable, with some sites showing an increase in U/Ca from March to May while other showed more stable values across seasons. Additionally, drip rates exhibit strong seasonal control, with peak rates in August 2023 (up to about 15 drips/min) and minimal rates in July 2024 ($<$1 drips/min in every site, with multiple dry sites), with Mg/Ca, Sr/Ca, and U/Ca tending to decrease with increased drip rates (Fig. 3.5).

Spatial differences show that the Grand Palace and Sunken Garden consistently show the highest Mg/Ca values (e.g., Grand Palace, May 2024: Mg/Ca = 1.59 mol/mol), while the Lodge Room tends to show the lowest (e.g., Lodge Room, October 2024: Mg/Ca = 0.075 mol/mol).

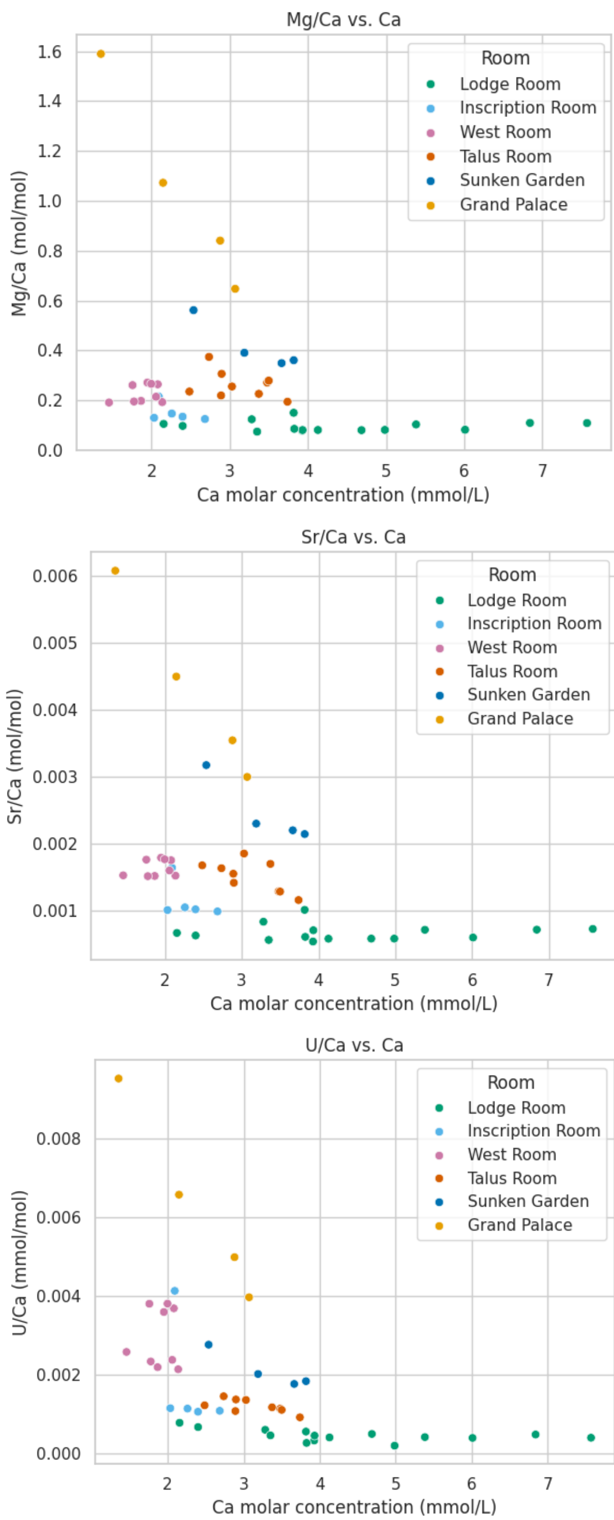

Figure 3.1: Mg/Ca (top), Sr/Ca (middle), and U/Ca (bottom) for drip waters collected from August 2023 to October 2024 compared to the Ca concentrations. Rooms within Lehman Caves are color-coded.

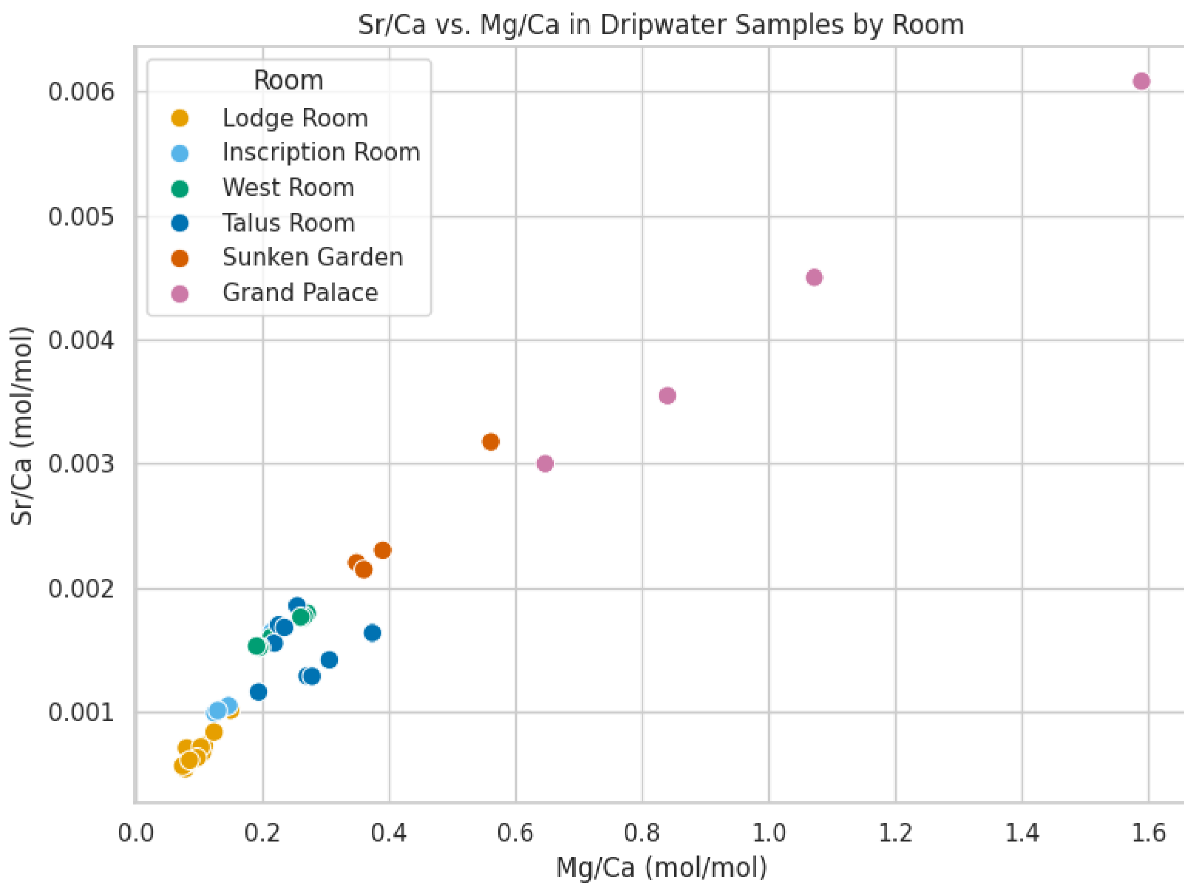

Figure 3.2: Mg/Ca vs Sr/Ca for the drip waters collected in Lehman Caves, showing a strong positive correlation.

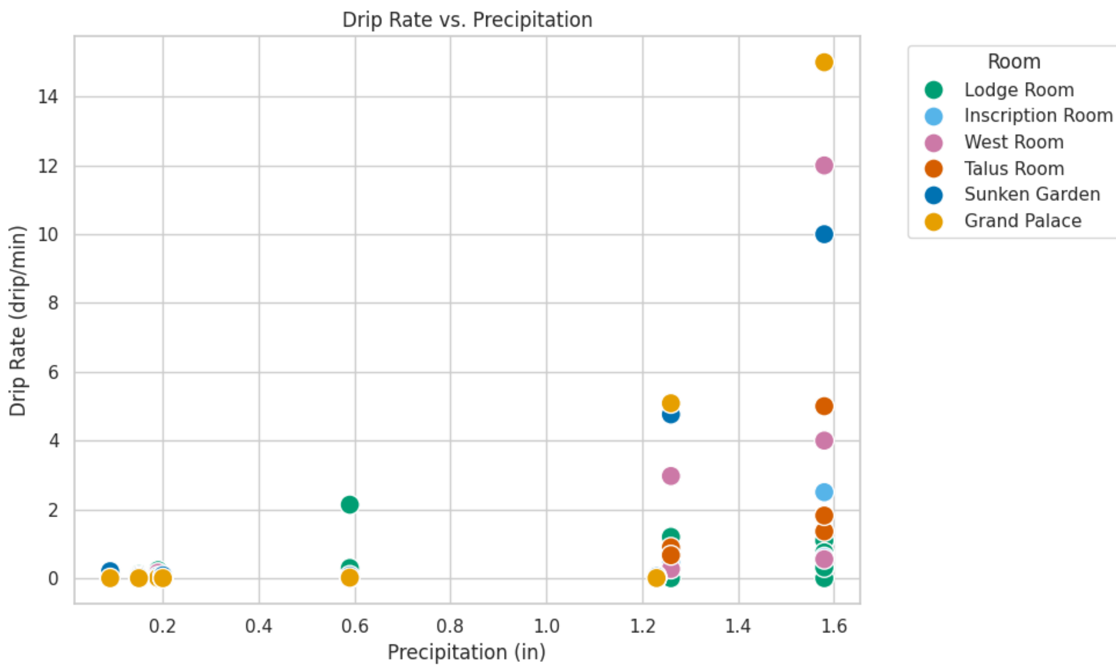

Figure 3.3: Drip rate versus precipitation for measured values in Lehman Cave sites, with each site color-coded. As precipitation increases, drip rate generally increases. With lower precipitation levels, many sample sites have low drip rates or are completely dry.

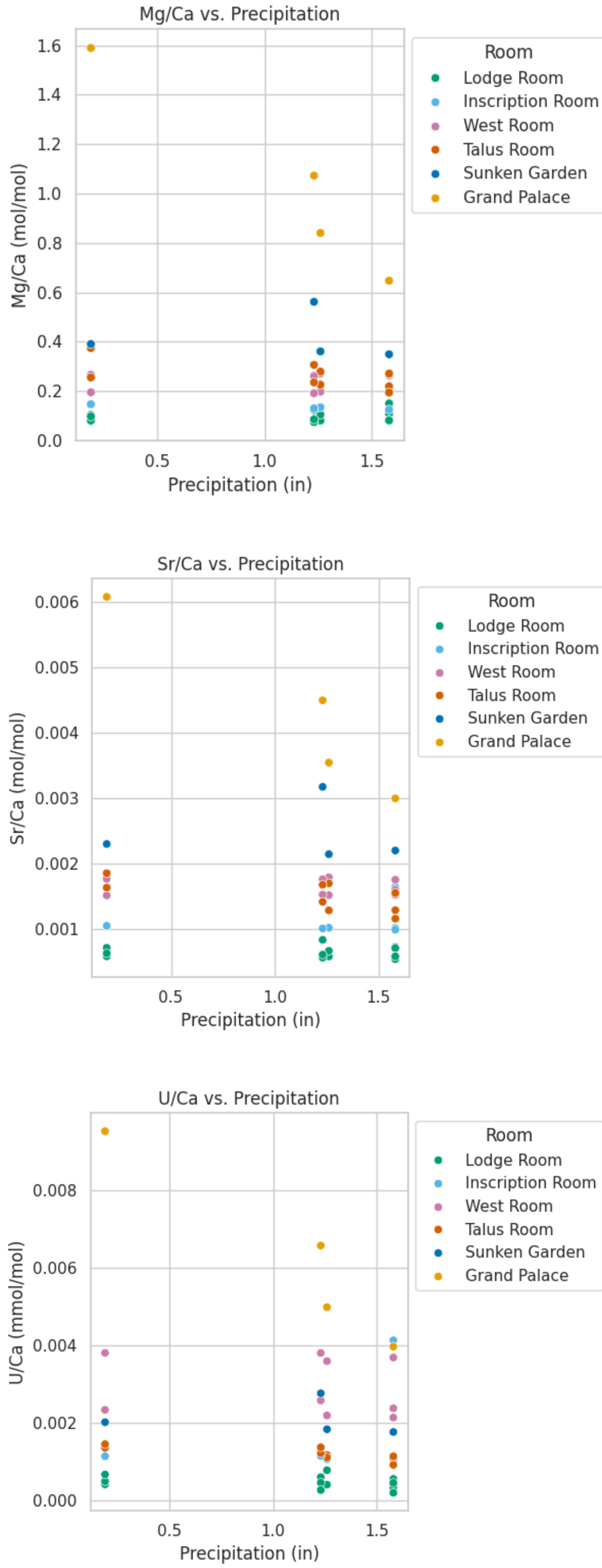

Figure 3.4: Mg/Ca (top), Sr/Ca (middle), and U/Ca (bottom) for drip waters collected from August 2023 to October 2024 compared to the month in which they were collected. Rooms within Lehman Caves are color-coded. As precipitation increases, trace element ratios generally decrease, indicating decreased PCP.

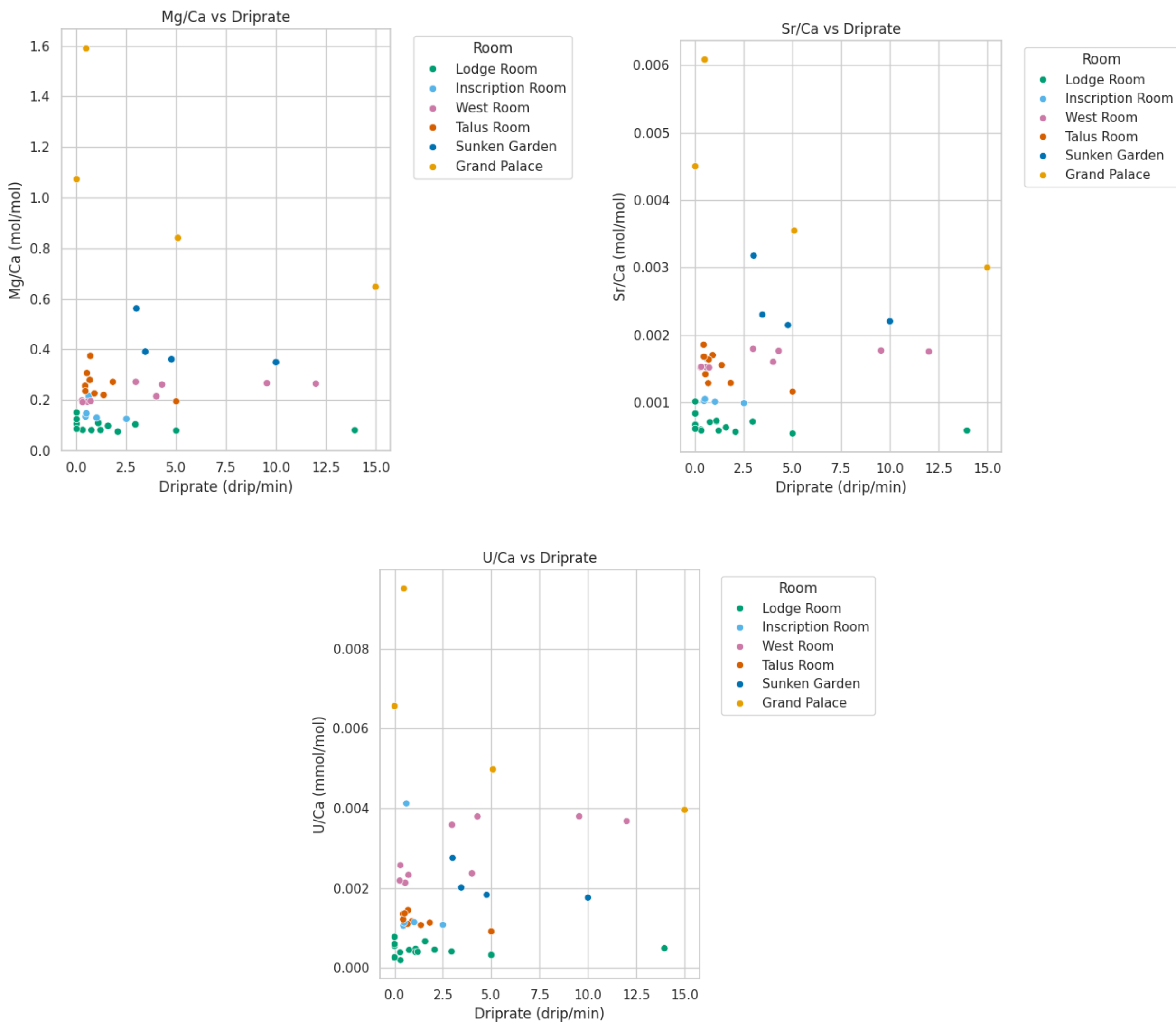

Figure 3.5: Mg/Ca (top), Sr/Ca (middle), and U/Ca (bottom) for drip waters collected from August 2023 to October 2024 plotted against drip rate in drips per minute. Different rooms in the cave are color-coded. As drip rate increases, Mg/Ca, Sr/Ca, and U/Ca tend to decrease.

Chapter 4

Discussion

4.1 Interpretation of trace element data

Some rooms have more stable drip water chemistry over the course of a year, while other rooms have greater changes throughout the year. In rooms that exhibit trace element ratio variability across the course of the year, Mg/Ca, Sr/Ca, and U/Ca values trend higher in drier months. In these drier months, drip rate tends to be lower. This signifies that the water residence times are higher in drier months, leading to increased PCP. As calcite precipitates, Ca is preferentially removed, enriching Mg, Sr, and U in the drip waters.

When comparing Mg/Ca, Sr/Ca, and U/Ca to Ca molar concentration, it appears that each room has its own "path" on the graphs. This could be due to differences in bedrock mineralogy (if the rock above the room is more Mg-rich or more Sr-rich, this could affect those ratios) or due to differing amounts of PCP (for example, if the epikarst was thicker above the room). From the map, it does not appear that the epikarst varies in thickness very much, but slight differences in thickness of the layer could have more of an effect than expected.

Sites that respond faster to environmental parameters like precipitation show large swings in geochemistry and drip rate over the course of a year, likely reflecting more direct flow paths of water from the surface to the cave. The Grand Palace is an example of such a room. Other sites appeared to maintain lower and more stable trace element ratios, which suggests consistent recharge and minimal PCP.

PCP is modeled here as Rayleigh fractionation of the drip waters (Fig. 4.1) [11]. The partition coefficient, D, for magnesium is typically between 0.01 and 0.1. The initial calcium value is defined as the highest concentration of calcium found in the drip waters sampled. The initial Mg/Ca ratio and initial D are found through best fit analysis.

The equation used for Rayleigh fractionation is:

$$(Mg/Ca_{solution})_f = (Mg/Ca_{solution})_0 f^{(D_{Mg}-1)} \tag{4.1}$$

in which $Mg/Ca_{[solution]})_0$ is the initial value of Mg/Ca, f is the fraction of calcium remaining, calculated as current calcium concentration over initial calcium concentration, and D is the partition coefficient for magnesium. The solution in this case is the drip water sample.

The Rayleigh modeling is also applied to Sr/Ca, as it is expected to undergo a similar PCP process as Mg/Ca (Fig. 4.2).

Mg/Ca and Sr/Ca were plotted against each other, with a PCP model line plotted alongside them (Fig. 4.3), with the equation:

$$Element/Ca = (Element/Ca_{initial} f^{(D-1)} \tag{4.2}$$

where $(\mathrm{Element/Ca})_{\mathrm{initial}}$ is the initial molar ratio before PCP, f is the fraction of Ca remaining in solution ($0 < f \leq 1$), and D is the partition coefficient for the element (e.g., $D_{\mathrm{Sr}} \approx 0.1$–$0.2$, $D_{\mathrm{Mg}} \approx 0.01$–$0.1$). The data points align well with the expected trend from the PCP.

When compared to previous studies of drip waters, the Mg/Ca ratios align well (Fig. 4.4). Here, we compare the samples of drip waters from this study to drip water samples from

Steponaitis (2015) [3]. The range of values of Mg/Ca ratios agree fairly well, while the Steponaitis values are skewed towards higher PCP. This is likely due to the collection period. The Steponaitis samples were collected during a very dry period, so many samples were collected from very slow drips or stagnant drops at the end of a stalactite, while the samples from this study were collected from active drips above fresh, modern calcite. The samples from this study are likely more representative of the type of drips that formed past stalagmites, as the drips have enough Ca left to actively form calcite, and eventually, a stalagmite beneath them.

Calcite samples from this study were also compared to stalagmites from Steponaitis (2015) (Fig. 4.5) [3]. The Mg/Ca values are largely similar, while the Sr/Ca values for the samples from this study are consistently higher than the Steponaitis values. There is one calcite sample from this study that has a significantly higher Mg/Ca ratio than the other samples. This sample should likely be retested to ensure accuracy.

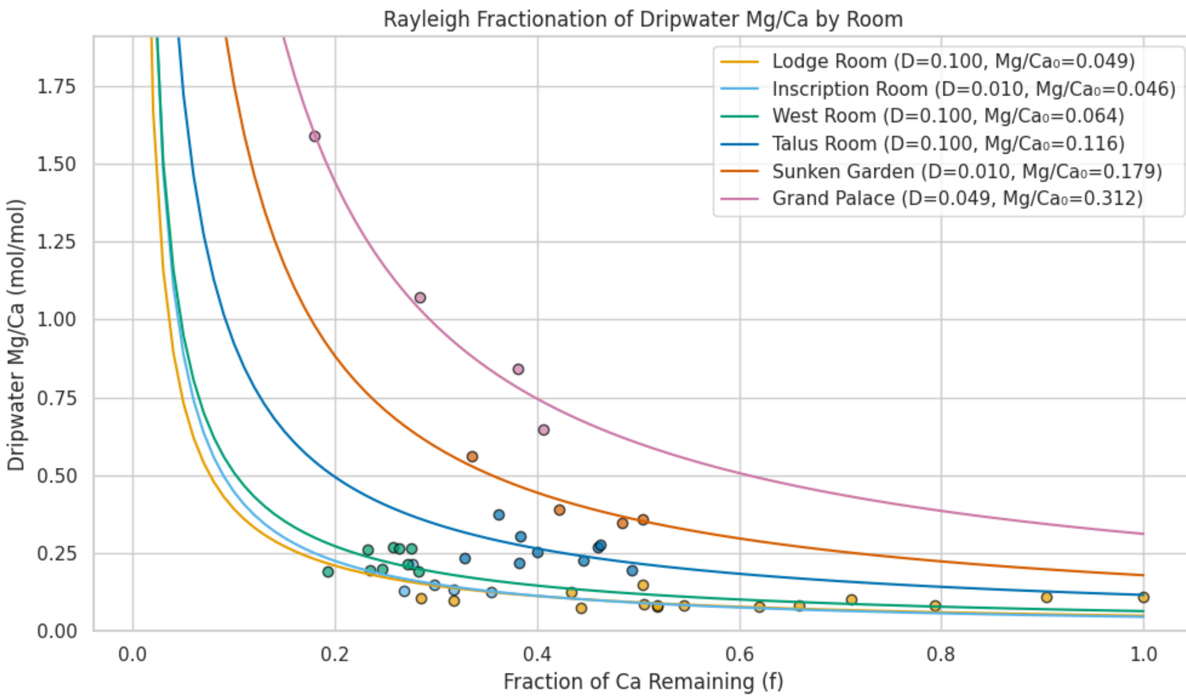

Figure 4.1: Rayleigh fractionation curves for magnesium for each room, with initial Ca concentration being the maximum Ca concentration found in the drip water, and partition coefficients and initial Mg/Ca calculated as best fit lines. Partition coefficients were constrained between 0.01 and 0.1.

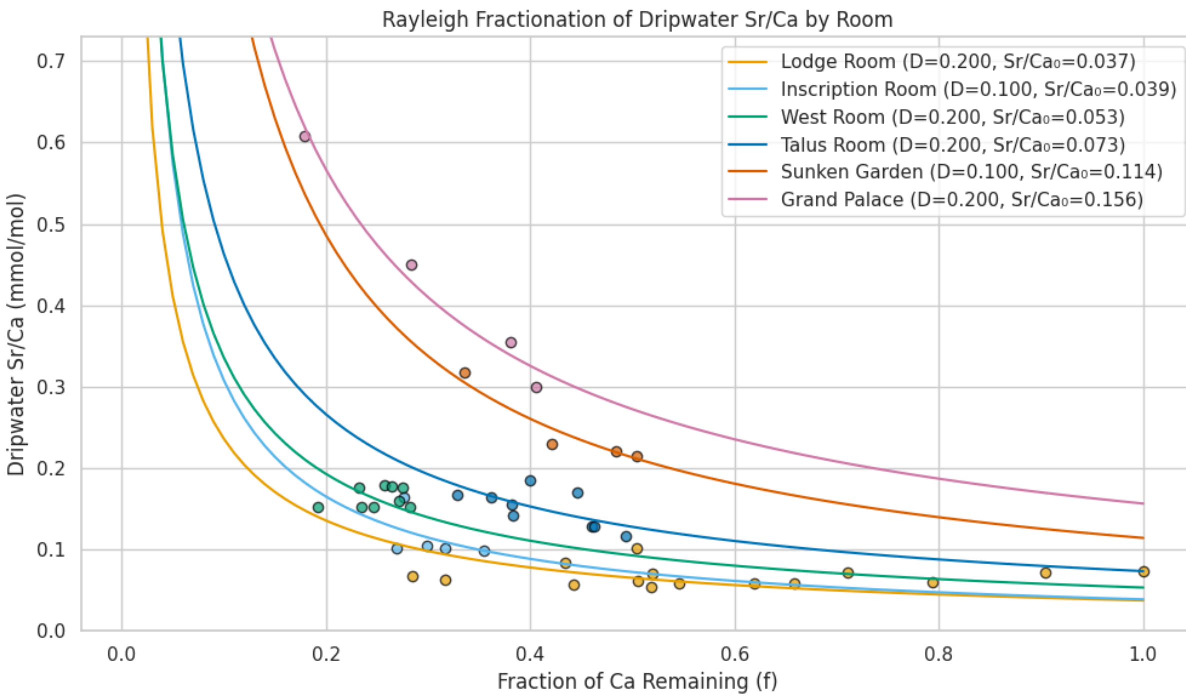

Figure 4.2: Rayleigh fractionation curves for strontium for each room, with initial Ca concentration being the maximum Ca concentration found in the drip water, and partition coefficients and initial Sr/Ca calculated as best fit lines. Partition coefficients were constrained between 0.1 and 0.2.

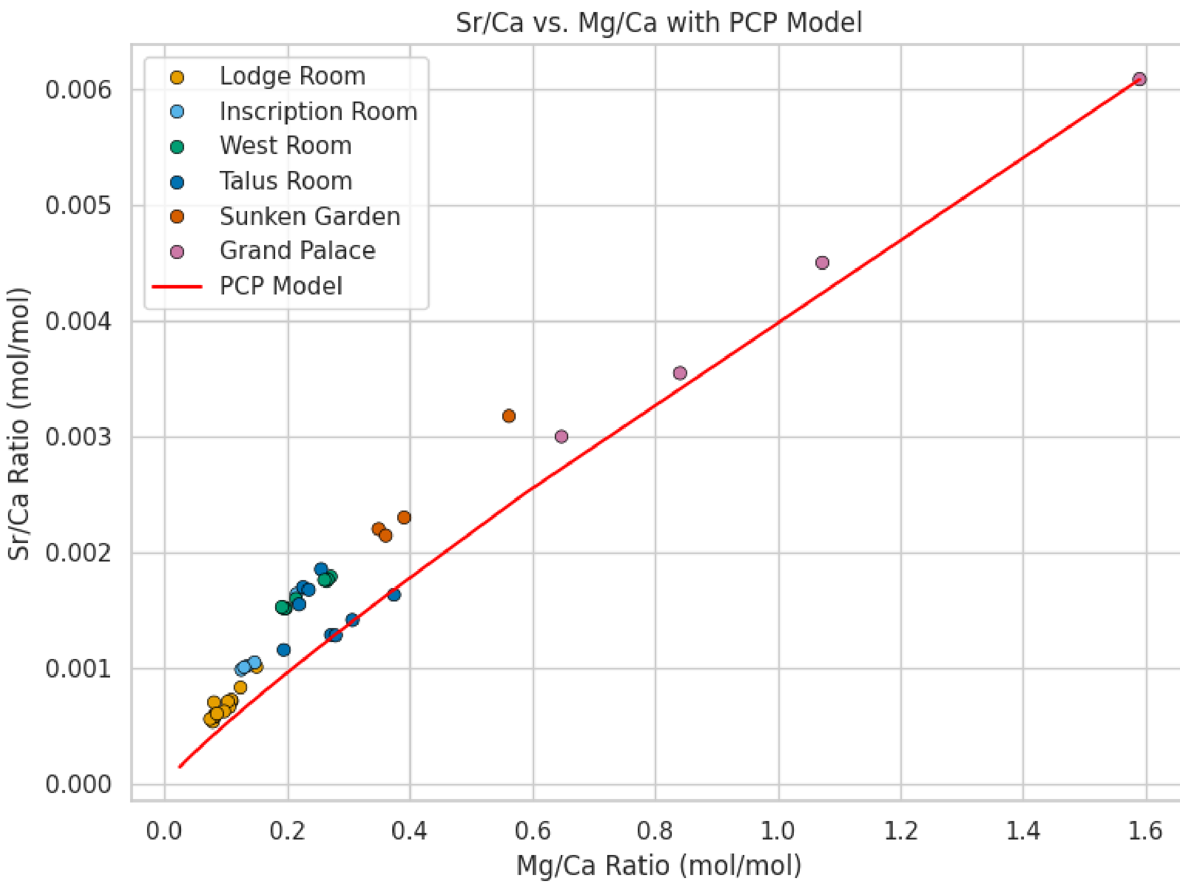

Figure 4.3: Mg/Ca vs. Sr/Ca, with a PCP model line. The data points align well with the expected trend from the PCP, indicating that PCP is a significant control on the trace element composition of the samples.

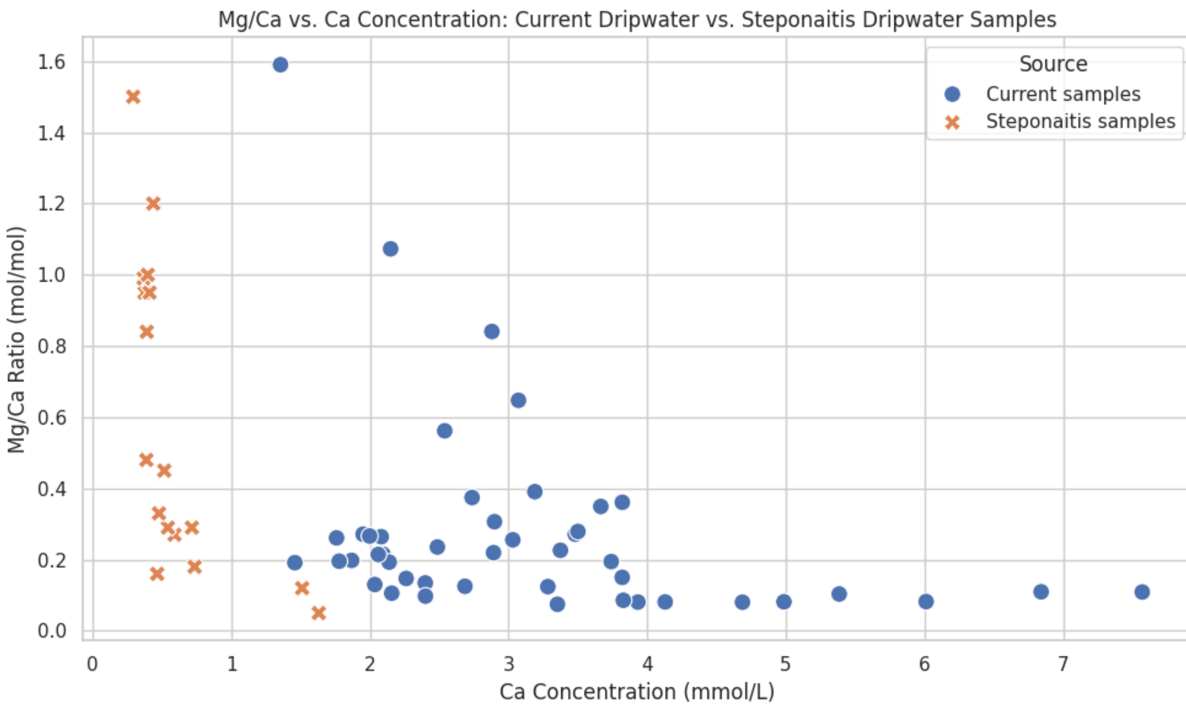

Figure 4.4: Mg/Ca vs Ca concentration, with samples from this study shown in blue circles and samples from Steponaitis (2015) shown in orange crosses [3]. The range of values of Mg/Ca ratios agree fairly well, indicating validity of the Mg/Ca values, while the Steponaitis values are skewed towards higher Sr/Ca.

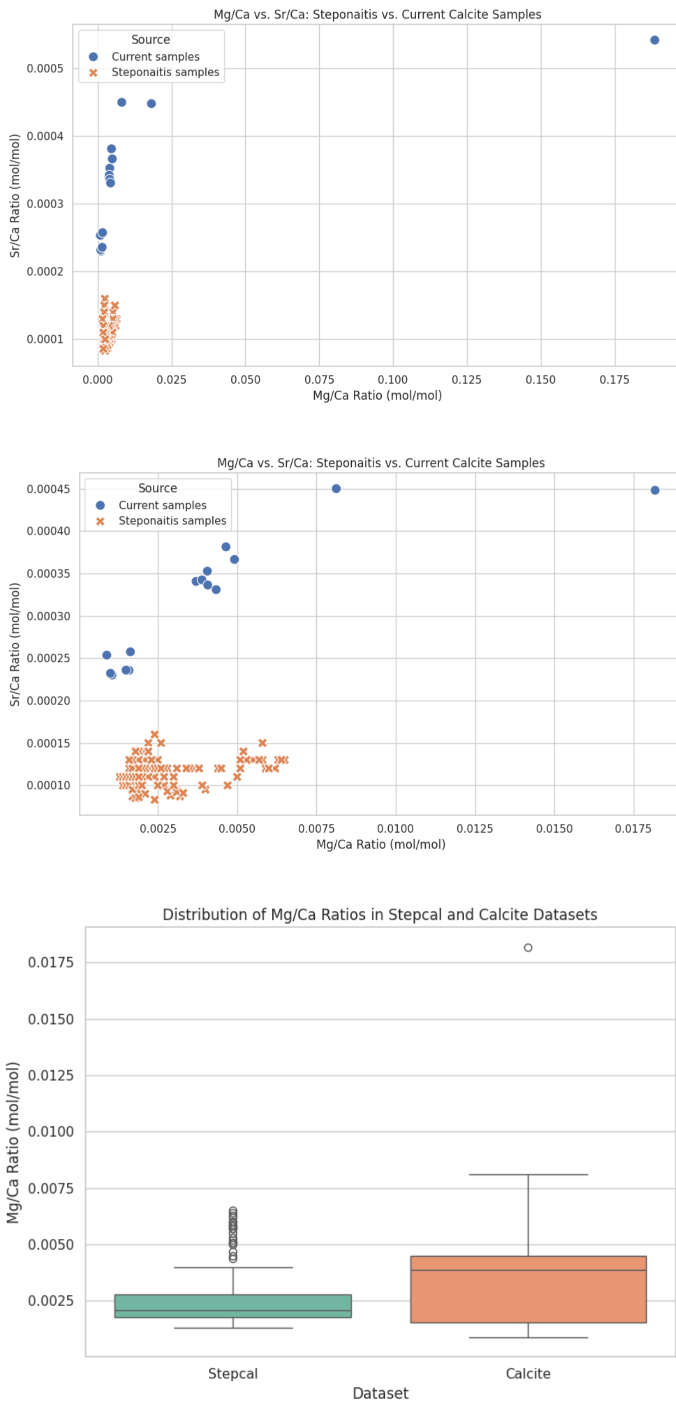

Figure 4.5: Calcite samples from this study compared to stalagmite samples from Steponaitis (2015) [3]. The Mg/Ca values are largely similar, while the Sr/Ca values for the samples from this study are consistently higher than the Steponaitis values. The top graph shows all of the values, while the middle graph removes the outlier to allow for closer view of the values. The bottom graph shows a box-and-whisker plot of the Mg/Ca ratio specifically, highlighting the general congruence of the two sample sets, with the outlier present in this study's sample set.

Chapter 5

Conclusion

This study reveals that drip water geochemistry at Lehman Caves varies both seasonally and spatially. It was expected that during drier months, PCP preferentially removes increased quantities of calcium from water as it passes through the epikarst, enriching the remaining solution in trace elements like magnesium and strontium. Elevated Mg/Ca, Sr/Ca, and U/Ca ratios observed during drier months and at sites with reduced drip rates align with the expected outcomes of intensified PCP processes during the water's path through the epikarst to the cave.

The variability in geochemical shifts across different cave rooms highlights the significance of spatial differences in karst systems. Factors such as bedrock lithology and thickness of the epikarst above a cave room can influence the extent of PCP, and consequently, the trace element composition of drip waters and the speleothems that precipitate. The spatial complexity shows that comprehensive sampling of various rooms within a cave is necessary in order to accurately interpret speleothem geochemical proxies.

The close alignment of drip water trace element ratios with PCP models indicates that trace element ratios in speleothems can serve as proxies for past hydrological conditions. However, the influence of cave-specific factors, such ventilation, humidity, and other conditions within the cave, can influence Mg/Ca and Sr/Ca ratios, causing changes within the precipitated speleothems. Therefore, further study is necessary to better understand the impact of these conditions on speleothem geochemical proxies. Additionally, further data collection and analysis is necessary to improve methods of understanding the relationship between drip waters and the trace element composition of calcite formed in caves. For instance, repeating this study in a region with larger variations of precipitation could show greater information about the effect of precipitation on drip water geochemistry. Finally, to gain a better sense of the uncertainty of the trace element values, replication of the sample measurements would be necessary.

Appendix A

Drip water Data

Site	Room	Date	Mg molar conc (mmol/L)	Ca molar conc (mmol/L)	Sr molar conc (mmol/L)	U molar conc (µmol/L)
1	Lodge	08/23	0.750365	6.842074	0.004916	0.003258
1	Lodge	08/23	0.825814	7.571638	0.005521	0.002987
2	Lodge	08/23	0.494332	6.012140	0.003613	0.002343
3	Lodge	08/23	0.573901	3.819493	0.003874	0.002103
4	Lodge	08/23	0.309767	3.927981	0.002126	0.001271
5	Lodge	08/23	0.318283	3.932548	0.002789	0.001763
6	Lodge	08/23	0.407014	4.986423	0.002915	0.000962
7	Inscription	08/23	0.450730	2.092490	0.003441	0.008627
8	Inscription	08/23	0.336234	2.684597	0.002660	0.002895
9	West	08/23	0.412722	2.137725	0.003260	0.004558
10	West	08/23	0.441869	2.059036	0.003299	0.004881
11	West	08/23	0.550212	2.080465	0.003652	0.007654
12	Talus	08/23	0.634985	2.890726	0.004491	0.003099
13	Talus	08/23	0.727959	3.740181	0.004341	0.003414
14	Talus	08/23	0.944652	3.480591	0.004489	0.003943
15	Sunken Garden	08/23	1.280568	3.664839	0.008074	0.006450
16	Grand Palace	08/23	1.988382	3.070952	0.009215	0.012162
4	Lodge	03/24	0.335566	4.129473	0.002409	0.001659
6	Lodge	03/24	0.227961	2.156220	0.001444	0.001670
8	Inscription	03/24	0.322799	2.398327	0.002451	0.002529
9	West	03/24	0.369618	1.866958	0.002839	0.004081
11	West	03/24	0.529368	1.949659	0.003497	0.006992
12	Talus	03/24	0.763265	3.373558	0.005739	0.003938
14	Talus	03/24	0.976856	3.499896	0.004505	0.003855
15	Sunken Garden	03/24	1.379069	3.820048	0.008200	0.006992
16	Grand Palace	03/24	2.420940	2.879374	0.010215	0.014332
1	Lodge	05/24	0.557238	5.385051	0.003858	0.002212
4	Lodge	05/24	0.377669	4.687066	0.002740	0.002301
6	Lodge	05/24	0.234239	2.399728	0.001514	0.001596
8	Inscription	05/24	0.332557	2.260398	0.002377	0.002564
9	West	05/24	0.347593	1.777081	0.002697	0.004141
11	West	05/24	0.532141	1.997299	0.003534	0.007587
12	Talus	05/24	0.774815	3.030030	0.005622	0.004100
14	Talus	05/24	1.024449	2.736192	0.004477	0.003958
15	Sunken Garden	05/24	1.246710	3.188955	0.007342	0.006419
16	Grand Palace	05/24	2.152264	1.353682	0.008232	0.012877
1	Lodge	10/24	0.407608	3.282887	0.002748	0.001959
4	Lodge	10/24	0.250215	3.351806	0.001893	0.001523
6	Lodge	10/24	0.328613	3.827405	0.002338	0.001006
8	Inscription	10/24	0.264621	2.033963	0.002057	0.002327
9	West	10/24	0.279107	1.457258	0.002230	0.003749
11	West	10/24	0.459041	1.758204	0.003102	0.006673
12	Talus	10/24	0.585168	2.485688	0.004174	0.003026
14	Talus	10/24	0.888255	2.897743	0.004112	0.003956
15	Sunken Garden	10/24	1.426263	2.538597	0.008064	0.006998
16	Grand Palace	10/24	2.304927	2.148367	0.009667	0.014103

Sample site	Room	Month	Year	Precipitation (in)	Drip rate (drip/min)
1	Lodge Room	August	2023	1.58	1.0900
1	Lodge Room	August	2023	1.58	1.0900
2	Lodge Room	August	2023	1.58	0.2900
3	Lodge Room	August	2023	1.58	0.0000
4	Lodge Room	August	2023	1.58	5.0000
5	Lodge Room	August	2023	1.58	0.7500
6	Lodge Room	August	2023	1.58	0.3100
7	Inscription Room	August	2023	1.58	0.6100
8	Inscription Room	August	2023	1.58	2.5000
9	West Room	August	2023	1.58	0.5500
10	West Room	August	2023	1.58	4.0000
11	West Room	August	2023	1.58	12.0000
12	Talus Room	August	2023	1.58	1.3600
13	Talus Room	August	2023	1.58	5.0000
14	Talus Room	August	2023	1.58	1.8200
15	Sunken Garden	August	2023	1.58	10.0000
16	Grand Palace	August	2023	1.58	15.0000
1	Lodge Room	March	2024	1.26	0.0000
4	Lodge Room	March	2024	1.26	0.0200
6	Lodge Room	March	2024	1.26	0.0000
8	Inscription Room	March	2024	1.26	0.0076
9	West Room	March	2024	1.26	0.0045
11	West Room	March	2024	1.26	0.0495
12	Talus Room	March	2024	1.26	0.0149
14	Talus Room	March	2024	1.26	0.0111
15	Sunken Garden	March	2024	1.26	0.0794
16	Grand Palace	March	2024	1.26	0.0847
1	Lodge Room	April	2024	0.59	0.1000
4	Lodge Room	April	2024	0.59	0.2941
6	Lodge Room	April	2024	0.59	2.1364
8	Inscription Room	April	2024	0.59	0.0177
9	West Room	April	2024	0.59	0.0039
11	West Room	April	2024	0.59	0.0532
12	Talus Room	April	2024	0.59	0.0169
14	Talus Room	April	2024	0.59	0.0114
15	Sunken Garden	April	2024	0.59	0.0779
16	Grand Palace	April	2024	0.59	0.0148
1	Lodge Room	May	2024	0.19	0.0492
4	Lodge Room	May	2024	0.19	0.2326
6	Lodge Room	May	2024	0.19	0.0263
8	Inscription Room	May	2024	0.19	0.0083
9	West Room	May	2024	0.19	0.0119
11	West Room	May	2024	0.19	0.1591
12	Talus Room	May	2024	0.19	0.0072

Sample site	Room	Month	Year	Precipitation (in)	Drip rate (drip/min)
14	Talus Room	May	2024	0.19	0.0116
15	Sunken Garden	May	2024	0.19	0.0575
16	Grand Palace	May	2024	0.19	0.0081
1	Lodge Room	June	2024	0.09	0.0222
4	Lodge Room	June	2024	0.09	0.1961
6	Lodge Room	June	2024	0.09	0.0172
8	Inscription Room	June	2024	0.09	0.0294
9	West Room	June	2024	0.09	0.0189
11	West Room	June	2024	0.09	0.1343
12	Talus Room	June	2024	0.09	0.0000
14	Talus Room	June	2024	0.09	0.0106
15	Sunken Garden	June	2024	0.09	0.2027
16	Grand Palace	June	2024	0.09	0.0000
1	Lodge Room	July	2024	0.15	0.0110
4	Lodge Room	July	2024	0.15	0.1176
6	Lodge Room	July	2024	0.15	0.0134
8	Inscription Room	July	2024	0.15	0.0000
9	West Room	July	2024	0.15	0.0000
11	West Room	July	2024	0.15	0.0800
12	Talus Room	July	2024	0.15	0.0108
14	Talus Room	July	2024	0.15	0.0106
15	Sunken Garden	July	2024	0.15	0.0414
16	Grand Palace	July	2024	0.15	0.0000
1	Lodge Room	September	2024	0.2	0.0026
4	Lodge Room	September	2024	0.2	0.0568
6	Lodge Room	September	2024	0.2	0.0063
8	Inscription Room	September	2024	0.2	0.0079
9	West Room	September	2024	0.2	0.0197
11	West Room	September	2024	0.2	0.0588
12	Talus Room	September	2024	0.2	0.0069
14	Talus Room	September	2024	0.2	0.0094
15	Sunken Garden	September	2024	0.2	0.0825
16	Grand Palace	September	2024	0.2	0.0000
1	Lodge Room	October	2024	1.23	0.0033
4	Lodge Room	October	2024	1.23	0.0345
6	Lodge Room	October	2024	1.23	0.0033
8	Inscription Room	October	2024	1.23	0.0169
9	West Room	October	2024	1.23	0.0051
11	West Room	October	2024	1.23	0.0714
12	Talus Room	October	2024	1.23	0.0074
14	Talus Room	October	2024	1.23	0.0087
15	Sunken Garden	October	2024	1.23	0.0500
16	Grand Palace	October	2024	1.23	0.0033

Appendix B

Calcite Data

Site	Room	Date Deployed	Date Collected	Relative Distance From Center of Plate	Mg Conc (mmol/L)	Ca Conc (mmol/L)	Sr Conc (mmol/L)	U Conc (µmol/L)
14	Talus Room	8/24/2023	3/5/2024	1	0.29884	64.30104	0.02452	0.16749
14	Talus Room	8/24/2023	3/5/2024	2	0.75423	203.56668	0.06933	0.50381
14	Talus Room	8/24/2023	3/5/2024	3	0.80425	198.04846	0.06985	0.41038
14	Talus Room	8/24/2023	3/5/2024	4	0.59312	152.45032	0.05220	0.39104
14	Talus Room	3/5/2024	10/3/2024	1	0.52789	129.60520	0.04359	0.36453
14	Talus Room	3/5/2024	10/3/2024	2	0.66405	153.08253	0.05065	0.41692
14	Talus Room	3/5/2024	10/3/2024	3	0.72050	146.54537	0.05371	0.32963
4	Lodge Room	8/24/2023	3/5/2024	1	0.20958	235.64527	0.05977	0.08821
4	Lodge Room	8/24/2023	3/5/2024	2	0.13441	127.40837	0.02933	0.06033
4	Lodge Room	8/24/2023	3/5/2024	3	0.14178	140.89169	0.03272	0.07416
4	Lodge Room	3/5/2024	10/3/2024	1	0.44739	273.81600	0.07053	0.13165
4	Lodge Room	3/5/2024	10/3/2024	2	0.07967	50.12365	0.01181	0.02728
4	Lodge Room	3/5/2024	10/3/2024	3	0.27711	185.11097	0.04368	0.11790
9	West Room	8/24/2023	3/5/2024	1	0.60048	3.18317	0.00172	0.01491
9	West Room	8/24/2023	3/5/2024	2	0.37013	45.54931	0.02050	0.11214
9	West Room	3/5/2024	10/3/2024	1	0.31904	17.54877	0.00786	0.04089

References

[1] D. Madsen, D. Rhode, D. Grayson, J. Broughton, S. Livingston, J. Hunt, J. Quade, D. Schmitt, and M. Shaver. "Late Quaternary environmental change in the Bonneville basin, western USA". In: *Palaeogeography, Palaeoclimatology, Palaeoecology* 167.3 (2001), pp. 243–271. ISSN: 0031-0182. DOI: https://doi.org/10.1016/S0031-0182(00)00240-6. URL: https://www.sciencedirect.com/science/article/pii/S0031018200002406.

[2] S. J. Patrickson, D. Sack, A. R. Brunelle, and K. A. Moser. "Late Pleistocene to early Holocene lake level and paleoclimate insights from Stansbury Island, Bonneville basin, Utah". In: *Quaternary Research* 73.2 (2010), pp. 237–246. DOI: 10.1016/j.yqres.2009.12.006.

[3] E. Steponaitis, A. Andrews, D. McGee, J. Quade, Y.-T. Hsieh, W. Broecker, B. Shuman, S. Burns, and H. Cheng. "Mid-Holocene drying of the U.S. Great Basin recorded in Nevada speleothems". In: *Quaternary Science Reviews* 127 (June 2015). DOI: 10.1016/j.quascirev.2015.04.011.

[4] J. D. Shakun, S. J. Burns, P. U. Clark, H. Cheng, and R. L. Edwards. "Milankovitch-paced Termination II in a Nevada speleothem?" In: *Geophysical Research Letters* 38 (2011). DOI: 10.1029/2011GL048560. URL: https://citeseerx.ist.psu.edu/document?repid=rep1&type=pdf&doi=83d71865f7253f5ccdfb280f80fdb19bd86d97ef.

[5] M. Lachniet, R. Denniston, Y. Asmerom, and V. Polyak. “Orbital control of western North America atmospheric circulation and climate over two glacial cycles”. In: *Nature communications* 5 (May 2014), p. 3805. DOI: 10.1038/ncomms4805.

[6] M. Cross, D. McGee, W. S. Broecker, J. Quade, J. D. Shakun, H. Cheng, Y. Lu, and R. L. Edwards. “Great Basin hydrology, paleoclimate, and connections with the North Atlantic: A speleothem stable isotope and trace element record from Lehman Caves, NV”. In: *Quaternary Science Reviews* 127 (Nov. 2015), pp. 186–198. DOI: 10.1016/j.quascirev.2015.06.016.

[7] J. S. Munroe and B. J. Laabs. “Latest Pleistocene history of pluvial Lake Franklin, northeastern Nevada, USA”. In: *GSA Bulletin* 125.3-4 (Jan. 2013), pp. 322–342. ISSN: 0016-7606. DOI: 10.1130/B30696.1. eprint: https://pubs.geoscienceworld.org/gsa/gsabulletin/article-pdf/125/3-4/322/418604/322.pdf. URL: https://doi.org/10.1130/B30696.1.

[8] B. Lehner, K. Verdin, and A. Jarvis. “New Global Hydrography Derived From Spaceborne Elevation Data”. In: *Eos Transactions, AGU* 89 (Mar. 2008), pp. 93–94. DOI: 10.1029/2008EO100001.

[9] Z. E. Havlena, L. D. Hose, H. R. DuChene, G. M. Baker, D. Powell, A. L. Labrado, B. Brunner, and D. S. Jones. “Origin and modern microbial ecology of secondary mineral deposits in Lehman Caves, Great Basin National Park, NV, USA”. In: *bioRxiv* (2023). DOI: 10.1101/2023.08.15.553329. eprint: https://www.biorxiv.org/content/early/2023/08/16/2023.08.15.553329.full.pdf. URL: https://www.biorxiv.org/content/early/2023/08/16/2023.08.15.553329.

[10] Weather Underground. *Monthly weather history for Baker, Nevada, August 2023 – October 2024*. Retrieved April 30, 2025. 2024. URL: https://www.wunderground.com/history/monthly/us/nv/baker/KCDC.

[11] "Geochemistry of Speleothems". In: *Speleothem Science*. John Wiley & Sons, Ltd, 2012. Chap. 8, pp. 245–289. ISBN: 9781444361094. DOI: https://doi.org/10.1002/9781444361094.ch8. eprint: https://onlinelibrary.wiley.com/doi/pdf/10.1002/9781444361094.ch8. URL: https://onlinelibrary.wiley.com/doi/abs/10.1002/9781444361094.ch8.